HHS Public Access

Author manuscript

Shock. Author manuscript; available in PMC 2016 September 01.

Published in final edited form as:

Shock. 2015 September ; 44(3): 258–264. doi:10.1097/SHK.0000000000000410.

Severe burn injury induces thermogenically functional mitochondria in murine white adipose tissue

Craig Porter[1,2], **David N. Herndon**[1,2], **Nisha Bhattarai**[1,2], **John O. Ogunbileje**[1,2], **Bartosz Szczesny**[3], **Csaba Szabo**[3], **Tracy Toliver-Kinsky**[3], and **Labros S. Sidossis**[1,4]

[1]Metabolism Unit, Shriners Hospitals for Children, Galveston, TX, USA

[2]Department of Surgery, University of Texas Medical Branch, Galveston, TX, USA

[3]Department of Anesthesiology, University of Texas Medical Branch, Galveston, TX, USA

[4]Department of Internal Medicine, University of Texas Medical Branch, Galveston, TX, USA

Abstract

Chronic cold exposure induces functionally thermogenic mitochondria in the inguinal white adipose tissue (iWAT) of mice. Whether this response occurs in pathophysiological states remains unclear. The purpose of this study was to determine the impact of severe burn trauma on iWAT mitochondrial function in mice. Male balb-c mice (10–12 weeks) received full-thickness scald burns to ~30% of the body surface area. iWAT was harvested from mice at 1, 4, 10, 20, and 40 days post injury. Total and uncoupling protein 1 (UCP1) dependent mitochondrial thermogenesis were determined in iWAT. Citrate synthase (CS) activity was determined as a proxy of mitochondria abundance. Immunohistochemistry was performed to assess iWAT morphology and UCP1 expression.

UCP1 dependent respiration was significantly greater at 4 and 10 days post burn compared to sham, peaking at 20 days post burn ($P<0.001$). CS activity was 3-fold greater at 4, 10, 20 and 40 days post-burn versus sham ($P<0.05$). Per mitochondrion, UCP1 function increased after burn trauma ($P<0.05$). After burn trauma, iWAT exhibited numerous multilocular lipid droplets which stained positive for UCP1.

The current findings demonstrate the induction of thermogenically competent mitochondria within rodent iWAT in a model of severe burn trauma. These data identify a specific pathology which induces the *browning* of WAT *in vivo*, and may offer a mechanistic explanation for the chronic hypermetabolism observed in burn victims.

Introduction

Severe burn trauma results in increased metabolic rate (1, 2), which can persist for months post injury in burn survivors (3). While increased ATP turnover explains some of the increase in metabolic rate seen in burn victims (4), a complete biochemical understanding of

Corresponding author: Craig Porter Ph.D., Metabolism Unit, Shriners Hospitals for Children – Galveston. Department of Surgery, University of Texas Medical Branch. Galveston, Texas, 77550. cr2porte@utmb.edu. P: 409-770-6676. F: 409-770-6674.

The authors have no conflicts of interest to disclose.

burn-induced hypermetabolism is currently lacking. Adrenergic stress, induced pharmacologically or by chronic cold exposure, results in mitochondrial biogenesis and the induction of uncoupling protein 1 (UCP1) in white adipose tissue (WAT) of rodents (5, 6). UCP1 is an inner mitochondrial membrane carrier protein that upon activation uncouples oxidative phosphorylation, causing mitochondrial membrane potential to be dissipated as heat (7). Recently, Shabalina and colleagues demonstrated that mitochondria within the inguinal WAT (iWAT) of mice exposed to chronic cold exposure become thermogenic, expressing fully functional UCP1 (8). These data (8) highlight the plasticity of iWAT in response to physiological stimulus.

Since burn trauma is associated with prolonged inflammatory (9, 10) and adrenergic stress (11–13), and a diminished capacity to thermoregulate (14, 15), we hypothesized that iWAT mitochondrial thermogenesis may contribute to burn-induced hypermetabolism. Indeed, others have reported an acute activation of intrascapular brown adipose tissue (BAT) in burned mice (16–18), supporting a role for adipose tissue mitochondrial thermogenesis in burn-induced hypermetabolism. In the current study, we used a murine model of burn trauma to determine the temporal relationship between iWAT mitochondrial thermogenesis and severe burns. We show for the first time that severe burn trauma results in the development of thermogenically competent mitochondria within iWAT of mice. These data have implications for the management of hypermetabolism in burn survivors.

Materials and methods

Animal procedures

All animal procedures were performed in line with the National Institutes of Health guidelines for experimental animal use. Permission to perform this study was obtained from the Institutional Animal Care and Use Committee at the University of Texas Medical Branch. Male BALB/c mice (10–12 weeks old) were used in the current study. Animals were housed at 24–26°C on a 12:12 light:dark cycle. Sham and burn treated mice underwent identical experimental procedures except for injury. Following an i.p. injection of 2 mg/kg buprenorphine, mice were anesthetized by inhalation of 3–5% isoflurane. Thereafter, ~40% of the dorsum was shaved with electrical clippers and ~ 1cc of lactated ringers (LR) solution was injected under the skin to protect the underlying spinal column. The dorsum of mice in the burn group was then exposed to ~95°C water for 10 sec to produce a full thickness scald wound covering 25–30% of the total body surface area (TBSA). Mice were then resuscitated with 1–2 cc of LR. We have previously used this rodent model to study the stress response to burn trauma (19–21). Further, similar to humans, others have shown that rodents develop hypermetabolism in response to burn trauma (18). Burn and sham treated mice were housed individually throughout the experimental period. Cohorts of mice were sacrificed at 1, 4, 10, 20, and 40 days post treatment. Both subcutaneous inguinal fat depots were harvested from each mouse for biochemical analysis.

Tissue analysis

Fat (iWAT) samples were divided into two portions after excision from the animal. One portion of iWAT was immediately submerged in an ice-cold preservation buffer (10mM

CaK_2-EGTA; 7.23mM K_2-EGTA; 20mM imidazole; 20mM taurine 50mM K-MES; 0.5mM dithithreitol; 6.56 $MgCl_2$; 5.77mM ATP and 15mM creatine phosphate (pH of 7.1)) for mitochondrial respiration measurements. Samples for mitochondrial respiration were stored in this buffer on ice until analysis. A second was preserved in 10% formalin for histology and immunohistochemistry.

High-resolution respirometry

Respirometry measurements were made within 30–180 mins after tissue was collected. Approximately twenty mgs of iWAT was blotted on filter paper and weighed on a precision micro-balance (Mettler-Toledo, Zaventem, Belgium). iWAT was then placed into an Oxygraph respirometer chamber (Oroboros Instruments, Innsbruck, Austria) with 2mls of pH adjusted (7.1) respiration buffer containing 0.5mM EGTA; 3mM $MgCl_2$; 60mM K-lactobionate; 20mM taurine; 10mM KH_2PO_4; 20mM HEPES; 110mM sucrose; 1mg/ml essential fatty acid free bovine serum albumin and 2μM digitonin. Each day, a background calibration was performed on polygraphic oxygen sensors at air saturation to ensure instrumental stability. Temperature was maintained at 37°C and O_2 concentration within the range of 200–400μM during all experiments. Mitochondrial O_2 flux was recorded at 2–4 sec intervals (DatLab, Oroboros Instruments, Innsbruck, Austria).

All respiratory states were determined sequentially within the same sample during a respirometry experiment typically lasting between 45–60 mins. iWAT mitochondrial respiratory capacity and function were assayed by the addition of substrates (1.5mM octanoyl-l-carnitine, 5mM pyruvate, 2mM malate, 10mM glutamate and 10mM succinate) followed by the titration of the UCP1 inhibitor guanosine-diphosphate (GDP) (to a final concentration of 30mM) (see Figure 1). This concentration of GDP was determined in pilot experiments were 5mM GDP was titrated into an Oxygraph chamber containing brown adipose tissue until no further reduction in respiration was seen. The titration of saturating levels of the UCP1 inhibitor GDP allowed the flux control ratio for GDP (FCR_{GDP}) to be calculated as an index of mitochondrial coupling control (equation 1) i.e., mitochondrial quality (22–24). Further, using respiration as a proxy of thermogenesis, this approach allowed total and UCP1 independent thermogenesis to be determined. UCP1 dependent thermogenesis was then quantified by subtracting UCP1 independent thermogenesis from total thermogenesis (equation 2). The use of GDP titrations provides a direct measure of UCP1 function per mg of tissue (8, 25–30). Moreover, calculating the FCR_{GDP} also provide a measure of UCP1 function per mitochondrion.

$$\mathrm{FCR_{GDP}} = \mathrm{UCP1\ independent\ thermogenesis / total\ thermogenesis.} \quad \text{(eq. 1)}$$

$$\mathrm{UCP1\ dependent\ thermogenesis} = \mathrm{total\ thermogenesis} - \mathrm{UCP1\ independent\ thermogenesis.} \quad \text{(eq. 2)}$$

Note: Total and UCP1 independent thermogenesis (i.e., respiration) were not corrected for residual (non-mitochondrial) respiration. Typically ~ 10% of tissue respiration is non-mitochondrial (31).

Citrate Synthase Activity

Citrate synthase (CS) activity was determined in iWAT samples as a proxy measure of mitochondrial volume density. As a key tricarboxylic acid cycle enzyme, CS activity correlates with mitochondrial respiratory capacity and mitochondrial volume in skeletal muscle (32), and is related to mitochondrial respiratory capacity in adipocytes (33). Briefly, approximately 20 mg of tissue was homogenized in ice-cold 175mM KCl buffer containing 2mM EDTA, 1% Triton and a protease inhibitor cocktail (Sigma-Aldrich, St Louis, MO) using a glass tissue grinder. iWAT lysates were centrifuged at 2000 rpm at 4°C and the supernatants were recovered and stored at −20°C until analysis. CS activity was determined spectrophotometrically using a modified version of the method of Sere (34). Lysates were diluted 1:10 in a TRIS-HCl buffer (110mM) containing 300μM acetyl-CoA (lithium salt) and a 100μM Et-OH solution of 5,5′-dithiobis-2-nitrobenzoic acid (DTNB). 500μM oxaloacetate was added to each well and UV light absorbance recorded at 412nM every 30 sec for a total of 10 mins (BioTek Eon™, Winooski, VT). The assay was performed at a pH of 8.1 at 37°C. The linear change in absorbance relating to the reaction of DTNB with free thiol groups (Coenzyme A) following the condensation of oxaloacetate and acetyl-CoA was used to calculate CS activity in μmol/g/min.

Histology and immunohistochemistry analysis

iWAT samples were embedded in paraffin and sectioned. After blocking with goat serum (rabbit IgG kit, Vector Laboratory, Burlingame, CA, USA) for 45 min, the sections were incubated with the primary antibody (rabbit anti-UCP1 antibody, Sigma u6382, Sigma-Aldrich, St. Louis, MO, USA) at a dilution of 1:1600 at 4°C. The following day, the sections were incubated with a secondary antibody (Rabbit IgG kit, Vector Laboratory, Burlingame, CA, USA), avidin-biotin - complex (ABC) solution, and then a diaminobenzidine solution (DAB peroxidase substrate kit, Vector Laboratory, Burlingame, CA, USA) at room temperature. Sections were washed in between each step with phosphate-buffered saline and Tween-20 (0.2%). iWAT images were captured using an Olympus BX41 light microscope.

Results

Mass specific thermogenesis

An Oxygraph trace of mass specific respiration for the sham, 1 and 10 days post burn groups is in shown in Figure 2A to demonstrate the clear difference in respiratory capacity and GDP sensitivity seen in iWAT from the 10 day post burn group. Total mitochondrial thermogenesis, shown in Figure 2B, was significantly elevated in iWAT of burned mice at 4 (15.8±1.9 pmol/sec/mg; $P<0.05$), 10 (17.1±2.2 pmol/sec/mg; $P<0.01$), 20 (20.3±2.5 pmol/sec/mg; $P<0.001$) and 40 (16.7±3.1 pmol/sec/mg; $P<0.05$) days post burn when compared to sham treated mice (7.1±1.1 pmol/sec/mg). In addition, total mitochondrial thermogenesis was significantly greater in iWAT of mice at 10 ($P<0.05$) and 20 ($P<0.01$) days post burn when compared to mice at 1 day post burn (8.5±1.3 pmol/sec/mg).

UCP1 independent thermogenesis (respiration following GDP titration) is presented in Figure 2C. Compared to sham (5.6±0.9 pmol/sec/mg), UCP1 independent thermogenesis was greater in the 20 (11.6±1.6 pmol/sec/mg; $P<0.05$) and 40 (11.8±2.0 pmol/sec/mg;

P<0.05) days post burn groups. No other statistical differences were detected between groups.

The flux control ratio for GDP (FCR_{GDP}) is shown in Figure 2D. The sham group was set to 1 (i.e. no change in respiration following GDP titration), and all burn groups were corrected for the GDP effect seen in sham mice. In comparison to sham (1.00), the FCR_{GDP} was significantly lower in iWAT at 10 (0.75±0.03; P<0.001) and 20 (0.79±0.04; P<0.001) days post burn. Similarly, the FCR_{GDP} was significantly lower in iWAT at 10 (P<0.001) and 20 (P<0.01) days post burn when compared to the 1 day post burn group (0.96±0.05). Finally, the FCR_{GDP} was significantly greater at 40 days post burn (0.93±0.02; P<0.05) when compared to 10 days post burn, indicating reversal of this effect with healing over time post-burn.

UCP dependent thermogenesis is shown in Figure 2E. When compared to sham, UCP1 dependent respiration was significantly greater in iWAT at 4 (5.4±0.8 pmol/sec/mg; P<0.05), 10 (7.6±1.0 pmol/sec/mg; P<0.001) and 20 (8.5±1.4 pmol/sec/mg; P<0.001) days post burn. In addition, UCP1 dependent respiration was significantly higher at 10 (P<0.001) and 20 (P<0.001) days post burn when compare to 1 day post burn (1.9±0.3 pmol/sec/mg).

Mitochondria specific thermogenesis

CS activity was determined in iWAT as a surrogate measure of mitochondrial protein abundance. CS activity data are presented in Figure 3A. iWAT CS activity significantly increased in a time dependent manner after burn trauma (P<0.05; Kruskal-Wallis test), peaking at 40 days post burn (294.5±82.2 nmol/g/sec) where CS activity was 3-fold greater than the sham group (134.7±24.0 nmol/g/sec; P<0.05).

An Oxygraph trace of mass specific respiration normalized to CS activity (i.e., mitochondrial specific respiration) for the sham, 1 and 10 days post burn groups is in shown in Figure 3B. Compared to the trace of mass specific respiration (see Figure 2A), the trace shown in Figure 3B demonstrates that the increase in respiratory capacity seen after burn trauma is largely the result of increase mitochondrial volume density. However, iWAT mitochondria are ~ 25% more sensitive to GDP a 10 days post burn compared to the sham and 1 days post burn group (as depicted previously in Figure 2D), highlighting qualitative mitochondrial adaptations in iWAT following burn trauma.

Normalizing mitochondrial respiratory fluxes to a marker of mitochondrial density such as CS activity provides a means to determine alterations in mitochondrial quality, which may be independent of changes in mitochondrial abundance. Total iWAT thermogenesis normalized to CS activity is presented in Figure 3C. No statistically significant differences were observed between groups, suggesting that increase in iWAT total respiratory capacity following burn trauma (see Figure 2B) is largely attributable to increased mitochondrial volume density. Similarly, UCP1 independent thermogenesis normalized to CS activity was similar between groups (Figure 3D), again suggesting that the increase in non UCP1 thermogenesis following burn trauma is the result of increased mitochondrial volume density. In contrast, when compared to both sham (14.8±3.3 * 10^{-3} pmol/sec/mg) and 1 day post burn (14.4±2.2 * 10^{-3} pmol/sec/mg), UCP1 dependent thermogenesis was significantly

greater in the 10 day post burn group (36.5±4.8 * 10^{-3} pmol/sec/mg) (Figure 3E). Further, UCP1 dependent thermogenesis was significantly lower at 40 days post burn (16.4±3.8 * 10^{-3} pmol/sec/mg; $P<0.05$) when compared to the 10 days post burn group (Figure 3E). This suggests the increase in iWAT UCP1 thermogenesis per gram of tissue seen after burn trauma is mediated in part by alterations in mitochondrial quality.

iWAT morphology and UCP1 expression

Representative histology sections (20X magnification) of iWAT stained for UCP1 are shown in Figure 4. Figure 4A shows iWAT images from a sham treated mouse (A1) and from burn treated mice at 1 (A2), 4 (A3), 10 (A4) and 20 (A5) days post burn. Pronounced UCP1 staining can clearly be seen in iWAT of burn treated mice, particularly at 10 and 20 days post burn. Moreover, the appearance of small multilocular lipid droplets is apparent from 1 day post burn, being most striking at 10 days post burn. In panel B1 and B2, enlarged images of iWAT from a sham and burn treated mouse are shown. While a small number of multilocular adipocytes can be seen in the iWAT of sham treated mice (B1), a plethora of these cells are seen in iWAT at 10 days post burn, suggesting that morphological changes in iWAT accompany the altered thermogenic function following burn trauma. 40X magnification of iWAT from a sham treated (C1) and a burned mouse at 4 (C2) 10 (C3) and 20 (C4) days post burn demonstrates the localization of UCP1 staining in and around multilocular adipocytes.

Discussion

Hypermetabolism, an increase in basal metabolic rate, is a hallmark of the stress response to burn trauma (1–3), and contributes to morbidity in burn survivors (35). While increased ATP demand accounts for approximately 50% of the hypermetabolic response to burns (4), a biochemical explanation for the remaining 50% is lacking. We hypothesized that burn trauma would induce thermogenically competent mitochondria within iWAT. Indeed, our data show that from 4 days post burn, UCP1 dependent mitochondrial thermogenesis is increased in iWAT, a response which peaked at 10 days post burn. This phenotypic switch of iWAT in response to burn trauma was mediated by mitochondrial biogenesis and UCP1 induction. These data suggest that iWAT mitochondrial thermogenesis may contribute to hypermetabolism in burn survivors.

Traditionally, brown adipose tissue (BAT) with its abundance of UCP1 positive mitochondria was thought to be found in distinct adipose tissue depots, separate from the more abundant WAT found subcutaneously and in the viscera. The work of Young and colleagues (6) demonstrating the appearance of BAT within the parametrial WAT of mice kept at 4°C for 4 weeks led to a paradigm shift, where it was apparent that BAT could be induced within adipose tissue depots normally considered as WAT, at least in rodents. This observation was confirmed by the work of Cousins and co-workers (5), who demonstrated the induction of BAT in various WAT depots of rats exposed to chronic cold exposure. Further, these researchers also showed that treatment with a β3-adrenoreceptor agonist also induced UCP1 expression within WAT, implicating adrenergic stress in this process. More recently, Zhang and colleagues (36) demonstrated in a murine model of severe burn trauma

that UCP1 mRNA was up regulated in WAT, suggesting that pathological conditions associated with adrenergic stress may induce thermogenic mitochondria within WAT.

Since burn trauma elicits a marked adrenergic stress response (2, 3, 11, 12), we theorized that a portion of the hypermetabolic response to burns may be attributable to the development of thermogenic mitochondria within WAT, especially when considering that β-blockade with propranolol blunts the hypermetabolic response to burn trauma (37–39). Indeed, O_2 consumption out-paces ATP production following burn trauma (4), suggesting that mitochondrial uncoupling (thermogenesis) contributes to burn-induced hypermetabolism. Our current data demonstrate that there is a marked increase in iWAT O_2 consumption following burn trauma. Specifically, we saw a ~2-fold increase in mitochondrial respiration uncoupled from ATP production at 4, 10 and 20 days after injury. While these data suggest greater iWAT thermogenic capacity post burn, this may merely reflect an increase in iWAT mitochondrial volume density. Since proton leaks occur in all mitochondrial inner membranes irrespective of the presence of uncoupling proteins, we determined mitochondrial thermogenesis before and after the addition of the UCP1 inhibitor GDP. This approach allows UCP1 mediated thermogenesis to be differentiated from basal inner mitochondrial proton conductance (25–27). While iWAT UCP1 independent respiration increased after burn, we saw a more pronounced increase in UCP1 dependent respiration post-burn. Specifically, there was a 4-fold increase in UCP1 dependent respiration in iWAT at 10 and 20 days post burn. These data provide direct evidence of a quantitative change in iWAT metabolic function in response to burns.

To address the impact of burn trauma on intrinsic mitochondria function in iWAT we calculated the flux control ratio for GDP (FCR_{GDP}). This measure provides an index of mitochondrial quality. We demonstrate a marked decrease in the FCR_{GDP} following burn trauma, meaning an increase in UCP1 function per mitochondrion in iWAT. These data indicate that there are adaptations in intrinsic mitochondrial function in iWAT following burn trauma, independent of changes in mitochondrial volume density. This response peaked at 10 days post burn and by 40 days post burn, when burn wounds had fully healed in these animals, iWAT mitochondrial UCP1 function was significantly different from that of animals at 10 days post burn. This observation highlights the plasticity of iWAT mitochondrial thermogenesis in response to burn trauma.

BAT differs from WAT in terms of both UCP1 function and mitochondrial volume density; thus, we determined CS activity as a surrogate of mitochondrial protein abundance (32, 33). In line with published data from cold exposure studies (5, 8, 40), we show a 2 to 3-fold increase in mitochondrial protein abundance (maximal CS activity) in iWAT after burn trauma. These data suggest that mitochondrial biogenesis is induced in iWAT in response to severe burns. A number of biochemical and stereological have been used as surrogates of mitochondrial volume density (32), which are often used to normalize mass specific measurements of ATP production or respiration to mitochondrial density (41–44). Using CS activity as a marker of mitochondrial volume density, we normalized our iWAT mitochondrial respiration data to CS activity, in order to report respiratory fluxes per unit of mitochondrial protein. Here, we show that greater total and UCP1 independent mitochondrial thermogenesis in iWAT following burn trauma are attributable to increased

mitochondrial volume density. In contrast, when normalized to mitochondrial volume density, UCP1 dependent mitochondrial thermogenesis remained greater in iWAT of burned mice. In particular, UCP1 dependent mitochondrial thermogenesis per mitochondrion was 3-fold greater in iWAT of mice at 10 days post burn when compared to sham, again suggesting that UCP1 activity per mitochondrion is increased in response to burn injury. It should be noted that this approach relies on the assumption that like muscle (32), CS activity is indeed a robust surrogate of mitochondrial volume density in WAT. However, increased UCP1 dependent thermogenesis normalized to CS activity after burn is in line with our FCR_{GDP} data, showing greater UCP1 function per mitochondrion. Interestingly, this response was reversible, where UCP1 dependent mitochondrial thermogenesis was significantly lower at 40 days post burn when compared to 10 days post burn. Again, this data underscores the temporal nature of this response, highlighting iWAT plasticity in response to burn trauma and healing.

In addition to strikingly different mitochondrial respiratory capacity and function, the morphology of BAT differs significantly from that of WAT. WAT adipocytes are typically larger and contain one lipid droplet which occupies almost all of the cell cytosol. In contrast, BAT adipocytes are small and multilocular in appearance (i.e. contain numerous lipid droplets). In the current study, we stained iWAT sections from sham and burn treated mice for UCP1 protein. Micrographs from these samples presented in Figure 4 show a clear reduction in adipocyte size and greater UCP1 protein content following burn trauma (Panels A1–A5). Further, while only a small number of multilocular cells could be seen in iWAT sections from sham treated mice (Panel B1), a plethora of these multilocular adipocytes where visible in iWAT sections from burned mice (Panel B2), suggesting that morphological adaptations in iWAT following burn trauma occur in concert with functional changes in mitochondrial thermogenic capacity. Moreover, when imaging iWAT sections at greater magnification, concurrent alterations in adipocyte morphology and UCP1 protein content can be clearly seen (Panels C1–C4), a response that again appears to be reversible. Collectively, these data support the notion that UCP1 protein content and function increase in iWAT in response to severe burn trauma, which is accompanied by pronounced alterations in adipocyte morphology. However, a limitation of the current study was that we did not have sufficient tissue to perform further microscopic analysis of our tissue. Future studies combining electron microscopy to image mitochondria and immunofluorescence to co-stain mitochondria with UCP1 would provide further support for our biochemical data demonstrating greater mitochondrial enzyme activity and UCP1 function.

To the best of our knowledge, we present the first evidence of *browning* of WAT following burn trauma, where we define *browning* as the development of a phenotype that is similar to BAT; specifically, increased UCP1 protein content and function, an increase in mitochondrial volume density and altered adipocyte morphology. Importantly, these adaptations augment mitochondrial thermogenesis. Previously, others have reported induction of UCP1 mRNA at 1, 2 and 3 days post injury in burned mice (36), however, caution should be exercised when interpreting UCP1 mRNA data, since there may be a discordance between UCP1 signal, protein levels, and ultimately function (45). While there is significant debate as to the genetic lineage of UCP1 positive adipocytes found in WAT

depots, our functional data suggest that these adipocytes contain thermogenically competent mitochondria; that is mitochondria with functional UCP1. While determining the lineage of these adipocytes was beyond the scope of the current study, based on the physiological significance of our data, we suggest that this may be insignificant, at least in the context of the hypermetabolic response to burns.

While little is known regarding the impact of burn induced *browning* of iWAT on whole body metabolism, Carter and colleagues demonstrated that cold exposure, burn trauma (30% TBSA) or skin excision (30% TBSA) led to comparable increases in glucose, fatty acid and acetate uptake within the intrascapular BAT of mice (16). Thus, it appears that these stressors result in similar increases in metabolic rate within UCP1 positive adipocytes. Further, these findings support the notion that UCP1 mediated thermogenesis following trauma such as burn and/or wound excision likely facilitates thermoregulation. Moreover, while there is around a 50% increase in glucose uptake within the heart of mice 24hr after a 25% TBSA scald burn, glucose uptake increases by ~350% in intrascapular BAT (17). These data further underscore the metabolic impact of activated UCP1 positive adipocytes in response to burn trauma. Further, while UCP1 positive adipocytes likely play an important role in the thermogenic component of burn-induced hypermetabolism, we have recently shown that skeletal muscle mitochondria become thermogenic in humans with severe burns (42), suggesting that multiple organs in the body likely contribute to this response. Intriguingly, recent data suggest that suppression of UCP1 protein in intrascapular BAT of burned mice blunts burn-induced hypermetabolism (18). Thus, future studies concerning the inhibition of UCP1 following severe burn trauma are warranted.

To summarize, we present novel data demonstrating the induction of thermogenically competent mitochondria within iWAT of mice in response to severe burn trauma. This *browning* of iWAT was the result of concurrent alterations in adipocyte morphology, mitochondrial volume density, and most strikingly, UCP1 function. These data are in line with those generated from cold exposure models, supporting a putative role for mitochondrial uncoupling in the thermoregulation of burn victims. Future studies should focus on confirming this phenomenon in human burn victims, while establishing the impact of environmental and pharmacological perturbators on WAT mitochondrial function following burn trauma.

Acknowledgments

This work was funded by the Shriners of America, The National Institute of Disability and Rehabilitation Research, and with the support of the Institute for Translational Sciences at the University of Texas Medical Branch, supported in part by a Clinical and Translational Science Award (UL1TR000071) from the National Center for Advancing Translational Sciences, National Institutes of Health.

We thank Geping Fang and Weihua Cui for assisting in animal care and husbandry and Dr. Manish K. Saraf for assistance in capturing immunohistochemistry images. We thank Dr. Sam Jacob, Dr. Robert Cox and Dr. Hal Hawkins of the Morphology and Pathology Core Facility at Shriners Hospitals for Children - Galveston for assistance in preparing slides for histology and immunohistochemistry. This work was funded by Shriners of North America research grants to L.S.S (84090 and 85310), T.T.K (85300), CS (85800), D.N.H (80500) and H.H (84060), and with the support of the Institute for Translational Sciences at the University of Texas Medical Branch, supported in part by a Clinical and Translational Science Award (UL1TR000071) from the National Center for Advancing Translational Sciences, National Institutes of Health. CP was supported by a postdoctoral research fellowship from the National Institute of Disability and Rehabilitation Research (H133P110012).

References

1. Goran MI, Peters EJ, Herndon DN, Wolfe RR. Total energy expenditure in burned children using the doubly labeled water technique. Am J Physiol. 1990; 259:576–85.
2. Wilmore D, Long J, Mason AJ, Skreen R, Pruitt BJ. Catecholamines: mediator of the hypermetabolic response to thermal injury. Ann Surg. 1974; 180:653–69. [PubMed: 4412350]
3. Jeschke MG, Gauglitz GG, Kulp GA, Finnerty CC, Williams FN, Kraft R, Suman OE, Mlcak RP, Herndon DN. Long-term persistance of the pathophysiologic response to severe burn injury. PLoS One. 2011; 6:e21245. [PubMed: 21789167]
4. Yu YM, Tompkins RG, Ryan CM, Young VR. The metabolic basis of the increase of the increase in energy expenditure in severely burned patients. JPEN J Parenter Enteral Nutr. 1999; 23:160–8. [PubMed: 10338224]
5. Cousin B, Cinti S, Morroni M, Raimbault S, Ricquier D, Pénicaud L, Casteilla L. Occurrence of brown adipocytes in rat white adipose tissue: molecular and morphological characterization. J Cell Sci. 1992; 103:931–42. [PubMed: 1362571]
6. Young P, Arch J, Ashwell M. Brown adipose tissue in the parametrial fat pad of the mouse. FEBS Lett. 1984; 167:10–4. [PubMed: 6698197]
7. Porter C, Malagaris I, Sidossis L. Is the heat surrounding adipose tissue mitochondria warranted? Curr Opin Clin Nutr Metab Care. 2014; 17:503–8. [PubMed: 25102333]
8. Shabalina I, Petrovic N, de Jong J, Kalinovich A, Cannon B, Nedergaard J. UCP1 in Brite/Beige Adipose Tissue Mitochondria Is Functionally Thermogenic. Cell Rep. 2013; 5:1196–203. [PubMed: 24290753]
9. Finnerty CC, Herndon DN, Przkora R, Pereira CT, Oliveira HM, Queiroz DM, Rocha AM, Jeschke MG. Cytokine expression profile over time in severely burned pediatric patients. Shock. 2006; 26:13–9. [PubMed: 16783192]
10. Gauglitz G, Song J, Herndon D, Finnerty C, Boehning D, Barral J, Jeschke M. Characterization of the inflammatory response during acute and post-acute phases after severe burn. Shock. 2008; 30:503–7. [PubMed: 18391855]
11. Jeschke MG, Chinkes DL, Finnerty CC, Kulp G, Suman OE, Norbury WB, Branski LK, Gauglitz GG, Mlcak RP, Herndon DN. Pathophysiologic response to severe burn injury. Ann Surg. 2008; 248:387–401. [PubMed: 18791359]
12. Norbury WB, Herndon DN, Branski LK, Chinkes DL, Jeschke MG. Urinary cortisol and catecholamine excretion after burn injury in children. J Clin Endocrinol Metab. 2008; 93:1270–5. [PubMed: 18211976]
13. Kulp GA, Herndon DN, Lee JO, Suman OE, Jeschke MG. Extent and magnitude of catecholamine surge in pediatric burned patients. Shock. 2010; 33:369–74. [PubMed: 20407405]
14. Caldwell FJ, Bowser B, Crabtree J. The effect of occlusive dressings on the energy metabolism of severely burned children. Ann Surg. 1981; 193:579–91. [PubMed: 7235763]
15. Caldwell FJ, Wallace B, Cone J, Manuel L. Control of the hypermetabolic response to burn injury using environmental factors. Ann Surg. 1992; 215:485–90. [PubMed: 1616385]
16. Carter E, Bonab A, Hamrahi V, Pitman J, Winter D, Macintosh L, Cyr E, Paul K, Yerxa J, Jung W, Tompkins R, Fischman A. Effects of burn injury, cold stress and cutaneous wound injury on the morphology and energy metabolism of murine brown adipose tissue (BAT) in vivo. Life Sci. 2011; 89:78–85. [PubMed: 21565200]
17. Carter E, Winter D, Tolman C, Paul K, Hamrahi V, Tompkins R, Fischman A. Combination of radiation and burn injury alters [^{18}F] 2-fluoro-2-deoxy-D-glucose uptake in mice. J Burn Care Res. 2012; 33:723–30. [PubMed: 23143615]
18. Yo K, Yu Y, Zhao G, Bonab A, Aikawa N, Tompkins R, Fischman A. Brown Adipose Tissue and Its Modulation by a Mitochondria-targeted Peptide in Rat Burn Injury Induced Hypermetabolism. Am J Physiol Endocrinol Metab. 2012; 304:331–41.
19. Bohannon J, Cui W, Sherwood E, Toliver-Kinsky T. Dendritic cell modification of neutrophil responses to infection after burn injury. J Immunol. 2008; 185:2847–53. [PubMed: 20679533]

20. Toliver-Kinsky T, Lin C, Herndon D, Sherwood E. Stimulation of hematopoiesis by the Fms-like tyrosine kinase 3 ligand restores bacterial induction of Th1 cytokines in thermally injured mice. Infect Immun. 2003; 71:3058–67. [PubMed: 12761083]
21. Toliver-Kinsky T, Varma T, Lin C, Herndon D, Sherwood E. Interferon-gamma production is suppressed in thermally injured mice: decreased production of regulatory cytokines and corresponding receptors. Shock. 2002; 18:322–30. [PubMed: 12392275]
22. Gnaiger E. Capacity of oxidative phosphorylation in human skeletal muscle: new perspectives of mitochondrial physiology. Int J Biochem Cell Biol. 2009; 41:1837–45. [PubMed: 19467914]
23. Gnaiger, E. An introduction to OXPHOS analysis. 4. OROBOROS MiPNet Publications; 2014. Mitochondrial pathways and respiratory control. Mitochondr Physiol Network 19.12
24. Pesta D, Gnaiger E. High-resolution respirometry: OXPHOS protocols for human cells and permeabilized fibers from small biopsies of human muscle. Methods Mol Biol. 2012; 810:25–58. [PubMed: 22057559]
25. Cannon B, Nedergaard J. Studies of thermogenesis and mitochondrial function in adipose tissues. Methods Mol Biol. 2001; 456:109–21. [PubMed: 18516556]
26. Cannon B, Nedergaard J. Respiratory and thermogenic capacities of cells and mitochondria from brown and white adipose tissue. Methods Mol Biol. 2001; 155:295–303. [PubMed: 11293080]
27. Cannon B, Nedergaard J. Nonshivering thermogenesis and its adequate measurement in metabolic studies. J Exp Biol. 2011; 214:242–53. [PubMed: 21177944]
28. Matthias A, Ohlson K, Fredriksson J, Jacobsson A, Nedergaard J, Cannon B. Thermogenic Responses in brown fat cells are fully UCP1-dependent. Journal of Biological Chemistry. 2000; 275:25073–81. [PubMed: 10825155]
29. Cannon B, Nedergaard J. Brown adipose tissue: function and physiological significance. Physiol Rev. 2004; 84:277–359. [PubMed: 14715917]
30. Nedergaard J, Matthias A, Golozoubova V, Jacobsson A, Cannon B. UCP1: The original uncoupling protein - and perhaps the only one? Journal of Bioenergetics and Biomembranes. 1999; 31:475–91. [PubMed: 10653476]
31. Rolfe D, Brown G. Cellular energy utilization and molecular origin of standard metabolic rate in mammals. Physiol Rev. 1997; 77:731–58. [PubMed: 9234964]
32. Larsen S, Nielsen J, Hansen CN, Nielsen LB, Wibrand F, Stride N, Schroder HD, Boushel R, Helge JW, Dela F, Hey-Mogensen M. Biomarkers of mitochondrial content in skeletal muscle of healthy young human subjects. J Physiol. 2012; 590:3349–60. [PubMed: 22586215]
33. Yin X, Lanza I, Swain J, Sarr M, Nair K, Jensen M. Adipocyte mitochondrial function is reduced in human obesity independent of fat cell size. J Clin Endocrinol Metab. 2014; 99:209–16.
34. Srere P. Citrate Synthase. Methods Enzymol. 1969; 13:3–11.
35. Hart DW, Wolf SE, Chinkes DL, Gore DC, Mlcak RP, Beauford RB, Obeng MK, Lal S, Gold WF, Wolfe RR, Herndon DN. Determinants of skeletal muscle catabolism after severe burn. Ann Surg. 2000; 232:455–65. [PubMed: 10998644]
36. Zhang Q, Ma B, Fischman A, Tompkins R, Carter E. Increased uncoupling protein 1 mRNA expression in mice brown adipose tissue after burn injury. J Burn Care Res. 2008; 29:358–62. [PubMed: 18354294]
37. Herndon D, Nguyen T, Wolfe R, Maggi S, Biolo G, Muller M, Barrow R. Lipolysis in burned patients is stimulated by the beta 2-receptor for catecholamines. Arch Surg. 1994; 129:1301–4. [PubMed: 7986160]
38. Herndon D, Rodriguez N, Diaz E, Hegde S, Jennings K, Mlcak R, Suri J, Lee J, Williams F, Meyer W, Suman O, Barrow R, Jeschke M, Finnerty C. Long-term propranolol use in severely burned pediatric patients: a randomized controlled study. Ann Surg. 2012; 256:402–11. [PubMed: 22895351]
39. Herndon DN, Hart DW, Wolf SE, Chinkes DL, Wolfe RR. Reversal of catabolism by beta-blockade after severe burns. N Engl J Med. 2001; 345:1223–9. [PubMed: 11680441]
40. Young P, Wilson S, Arch J. Prolonged beta-adrenoceptor stimulation increases the amount of GDP-binding protein in brown adipose tissue mitochondria. Life Sci. 1984; 34:1111–7. [PubMed: 6323900]

41. Boushel R, Gnaiger E, Schjerling P, Skovbro M, Kraunsøe R, Dela F. Patients with type 2 diabetes have normal mitochondrial function in skeletal muscle. Diabetologia. 2007; 50:790–6. [PubMed: 17334651]

42. Porter C, Herndon D, Borscheim E, Chao T, Reidy P, Borack M, Rasmussen B, Chondonikola M, Saraf M, Sidossis L. Uncoupled skeletal muscle mitochondria contribute to hypermetabolism in severely burned adults. Am J Physiol Endocrinol Metab. 2014; 307:462–7.

43. Rabøl R, Larsen S, Højberg P, Almdal T, Boushel R, Haugaard S, Andersen J, Madsbad S, Dela F. Regional anatomic differences in skeletal muscle mitochondrial respiration in type 2 diabetes and obesity. J Clin Endocrinol Metab. 2010; 95:857–63. [PubMed: 20061415]

44. Short KR, Bigelow ML, Kahl J, Singh R, Coenen-Schimke J, Raghavakaimal S, Nair KS. Decline in skeletal muscle mitochondrial function with aging in humans. Proc Natl Acad Sci U S A. 2005; 102:5618–23. [PubMed: 15800038]

45. Nedergaard J, Cannon B. UCP1 mRNA does not produce heat. Biochim Biophys Acta. 2013

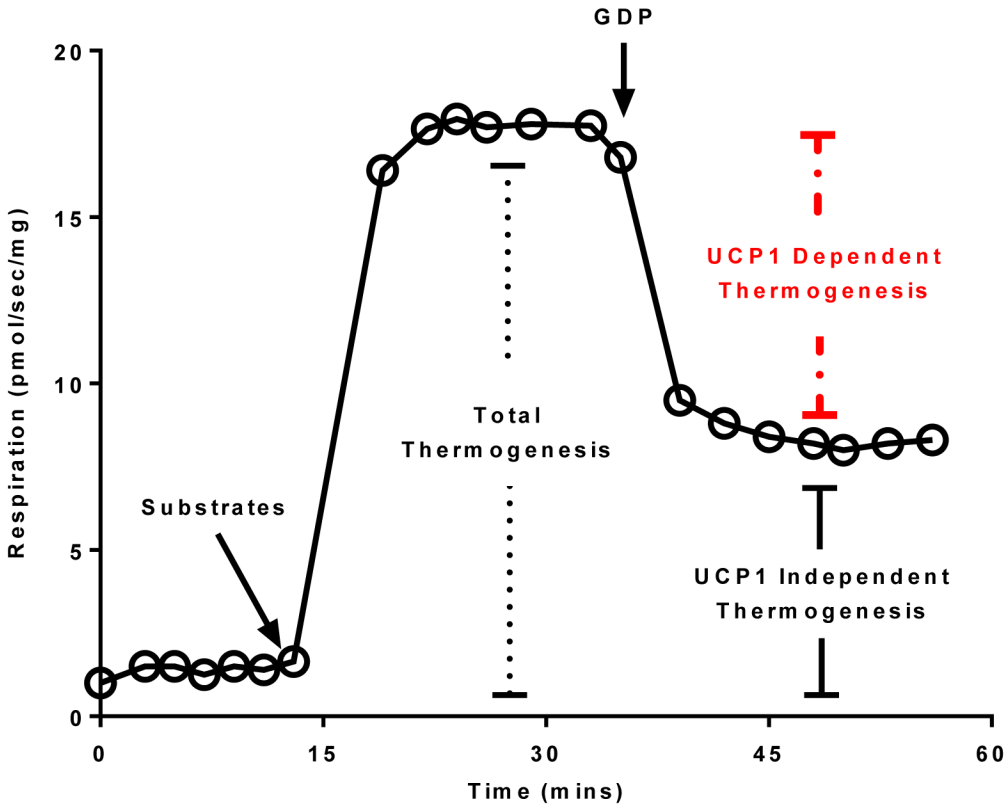

Figure 1.

Schematic representation of the mitochondrial respiration protocol employed in the current study. Steady state leak (uncoupled) respiration was determined before (total thermogenesis) and after (UCP1 independent respiration) the addition of the UCP1 inhibitor guanosine diphosphate (GDP). The difference between total and UCP1 independent thermogenesis represents UCP1 dependent thermogenesis.

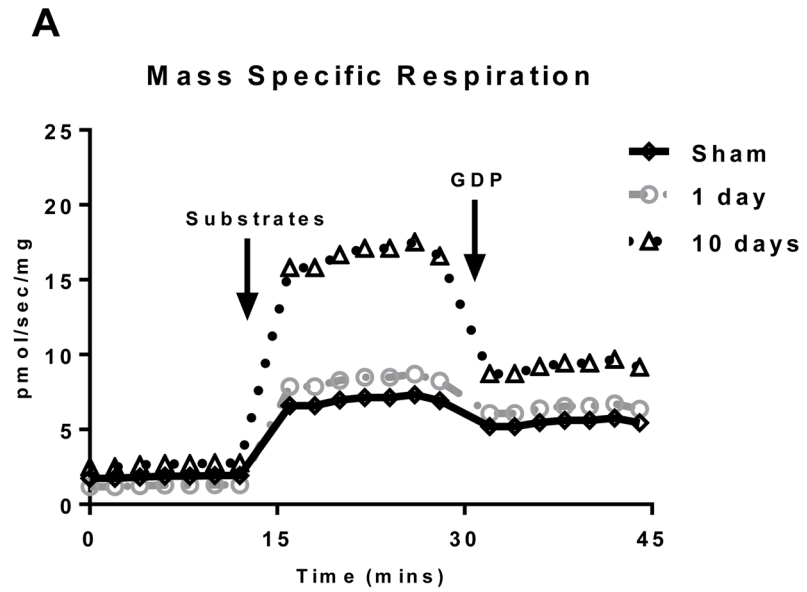

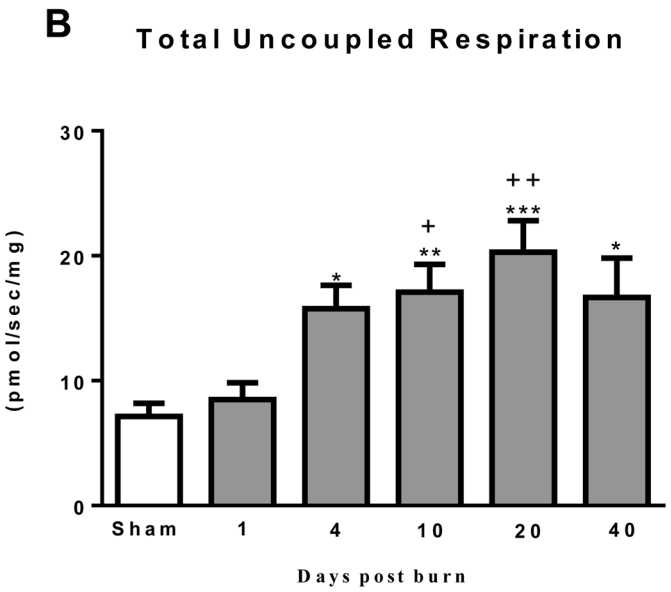

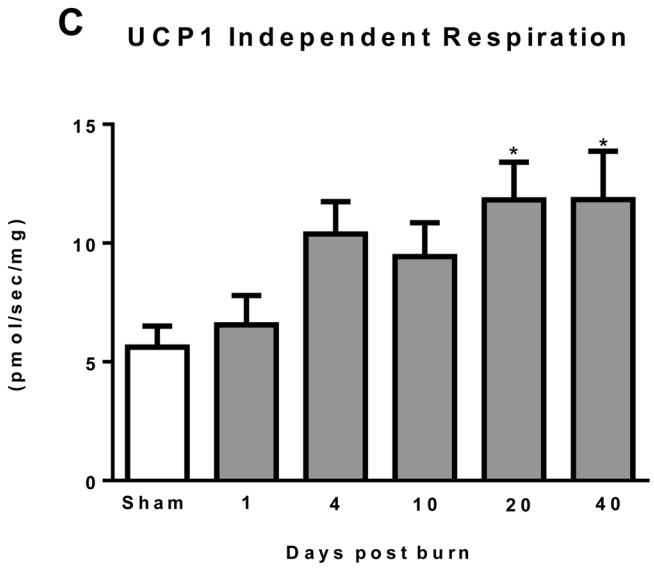

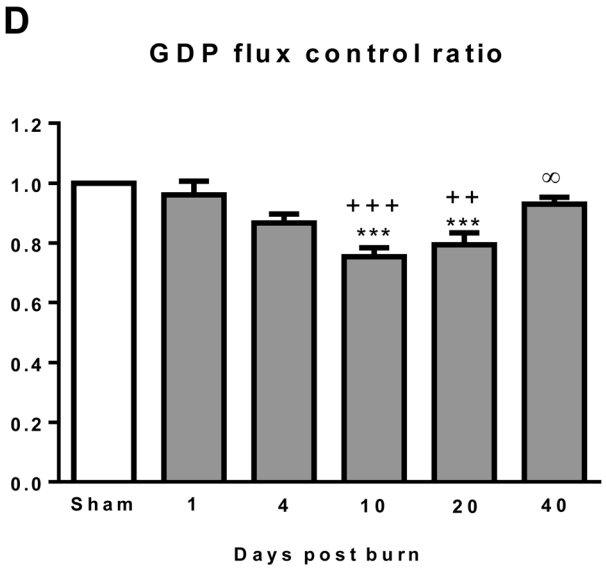

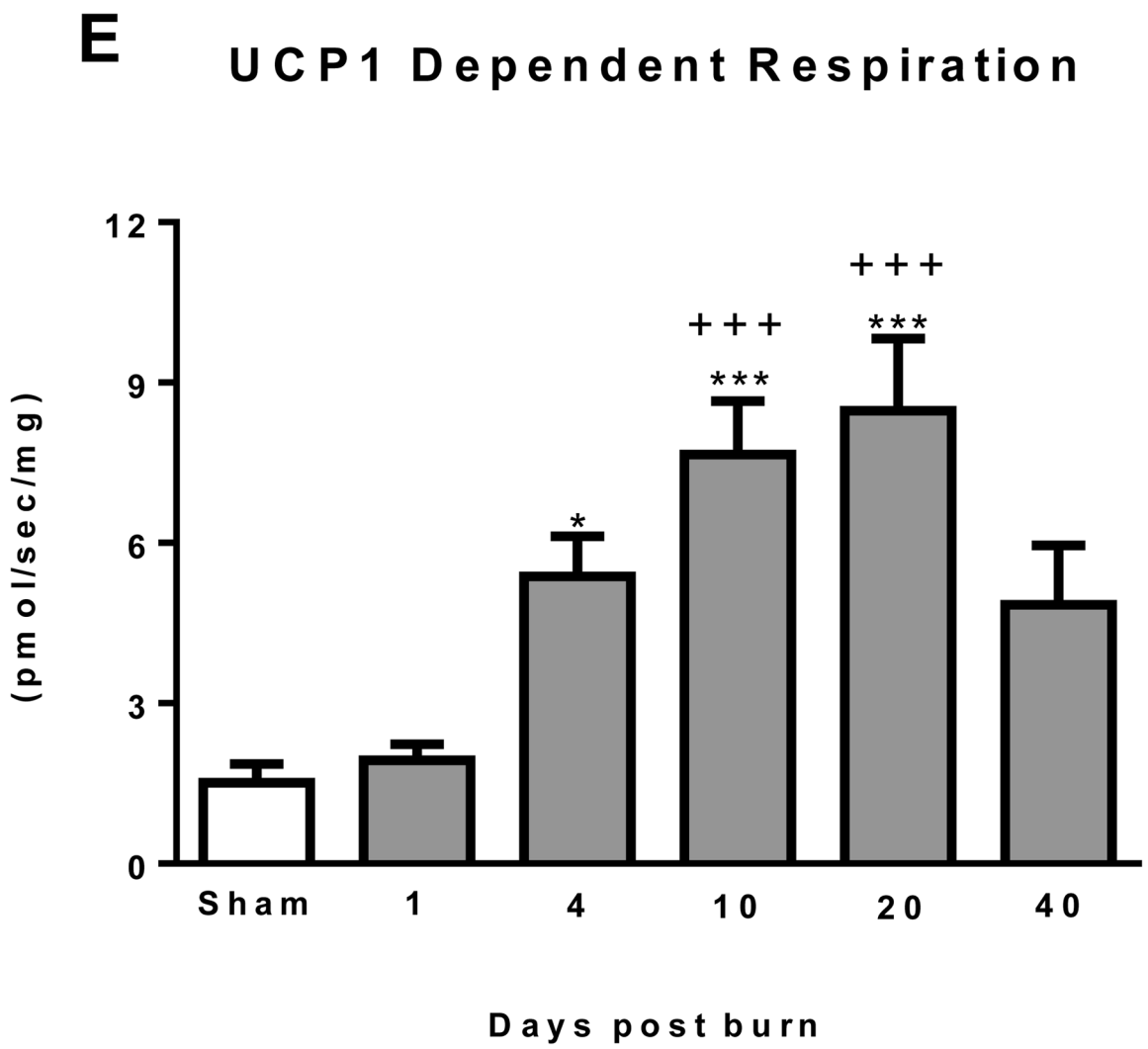

Figure 2.

(A) Representative Oxygraph traces for respirometry experiments showing mass specific respiratory fluxes following titration of substrates and then GDP. Group mean data from sham (n=10) 1 day post burn (n=8) and 10 days post burn (n=9) are plotted. (B) Total uncoupled respiration per mg of tissue after the addition of substrates increases after burn injury. (C) UCP1 independent respiration per mg of tissue following titration of GDP marginally increased after burn trauma. (D) GDP flux control ratio was reduced after burn injury, indicating greater GDP sensitivity and thus UCP1 function. (E) UCP1 dependent respiration per mg of tissue, i.e., the change in respiration after GDP titration significantly increased after burn trauma, demonstrating the induction of thermogenically competent mitochondria in iWAT following severe burns. DPB = days post burn. *P<0.05, **P<0.01 and ***P<0.001 vs. sham. $^{+}$P<0.05, $^{++}$P<0.01 and $^{+++}$P<0.001 vs. 1 DPB. ∞P<0.05 vs. 10 DPB.

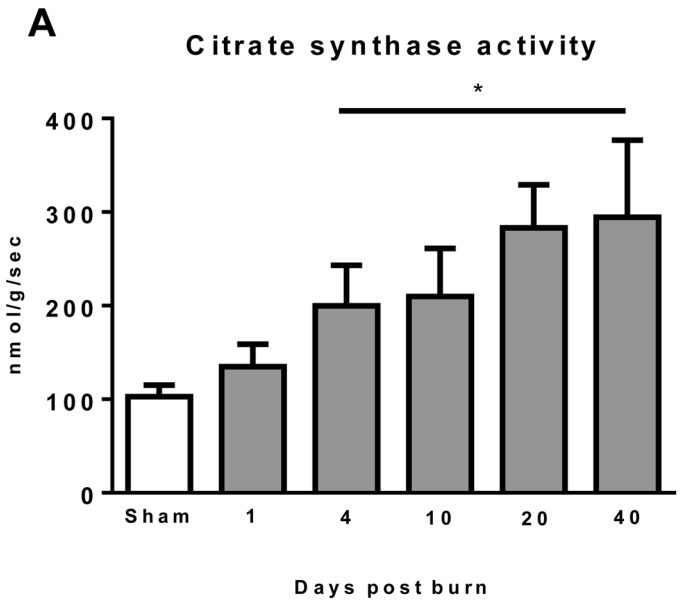

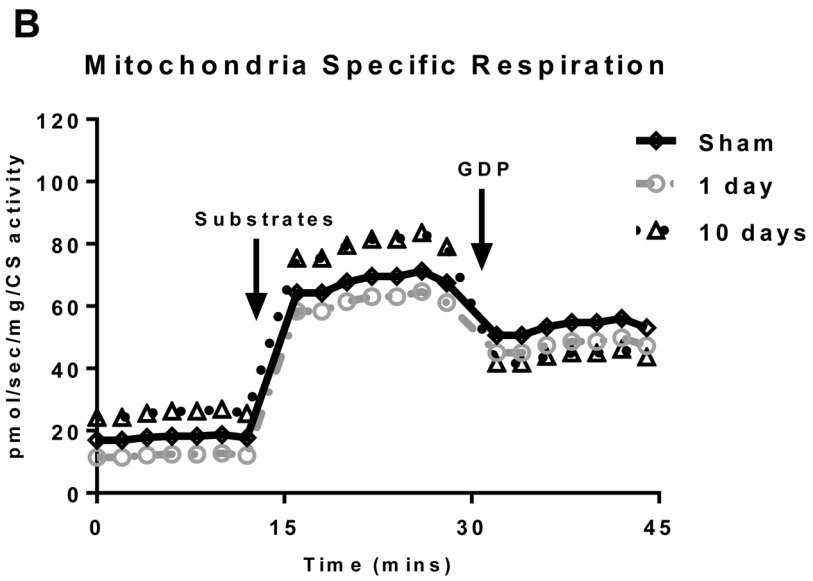

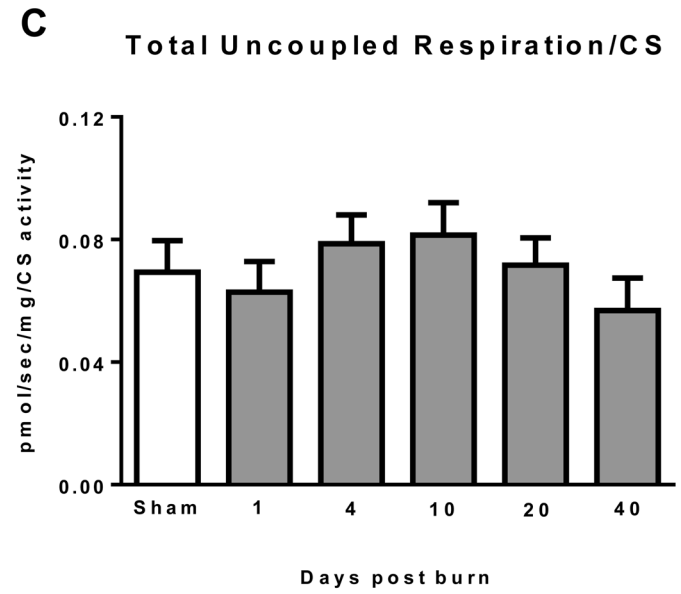

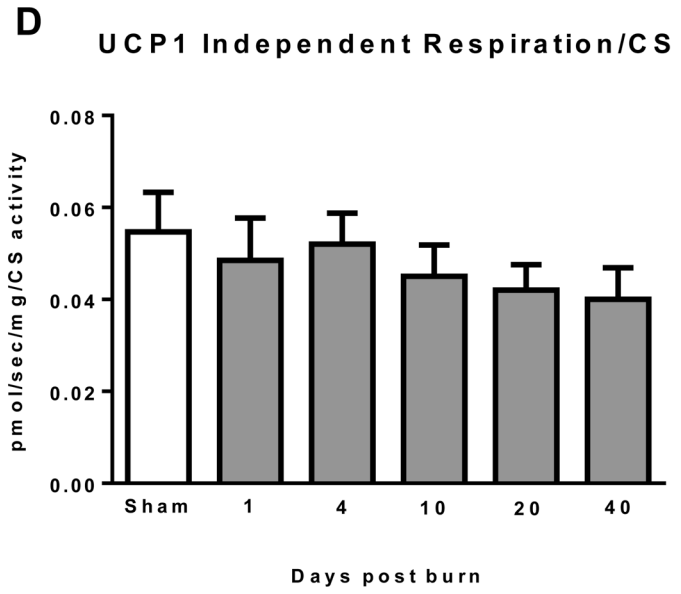

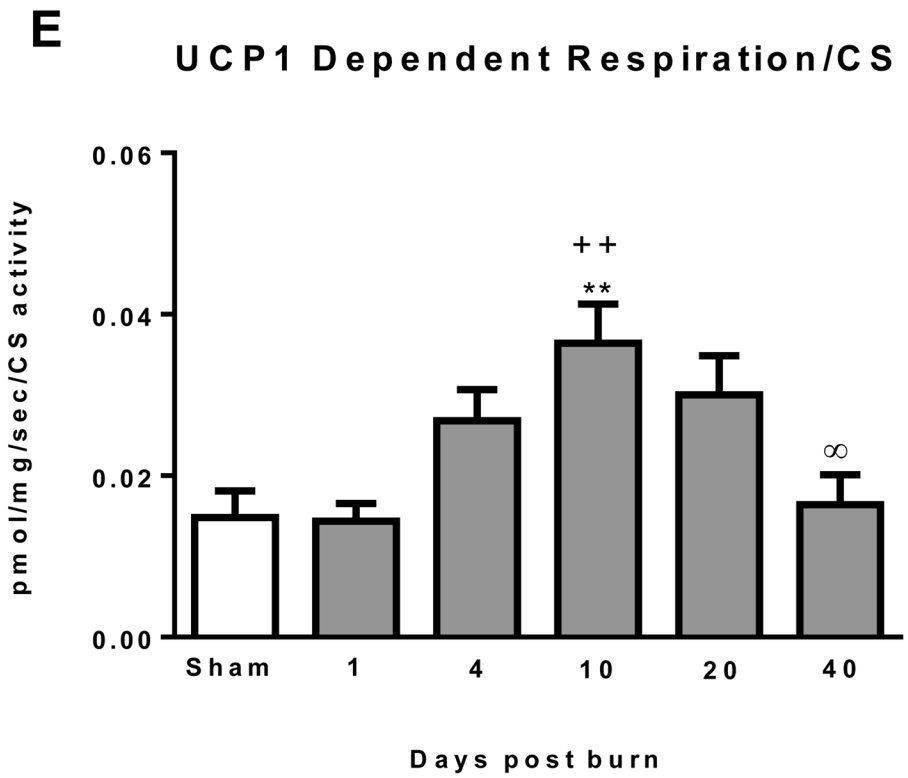

Figure 3.

(A) Citrate synthase (CS) activity increased in iWAT after burn indicating greater mitochondrial volume density. (B) Representative Oxygraph traces for respirometry experiments showing respiratory fluxes normalized to CS activity following titration of substrates and then GDP. Group mean data from sham (n=10) 1 day post burn (n=8) and 10 days post burn (n=9) are plotted. (C) Total uncoupled respiration normalized to CS activity was not altered by burn, indicating that greater iWAT respiratory capacity is largely attributable to greater mitochondrial volume density (D) UCP1 independent thermogenesis normalized to CS activity was similar across all groups, suggesting increased UCP1 independent respiration in iWAT post burn is the result of increased mitochondrial volume density. (E) UCP1 dependent respiration normalized to CS activity was significantly elevated post burn, indicating that intrinsic mitochondrial function is altered in iWAT after severe burn trauma. DPB = days post burn. *P<0.05 and **P<0.01 vs. sham. $^{++}$P<0.01 vs. 1 DPB. ∞P<0.05 vs. 10 DPB.

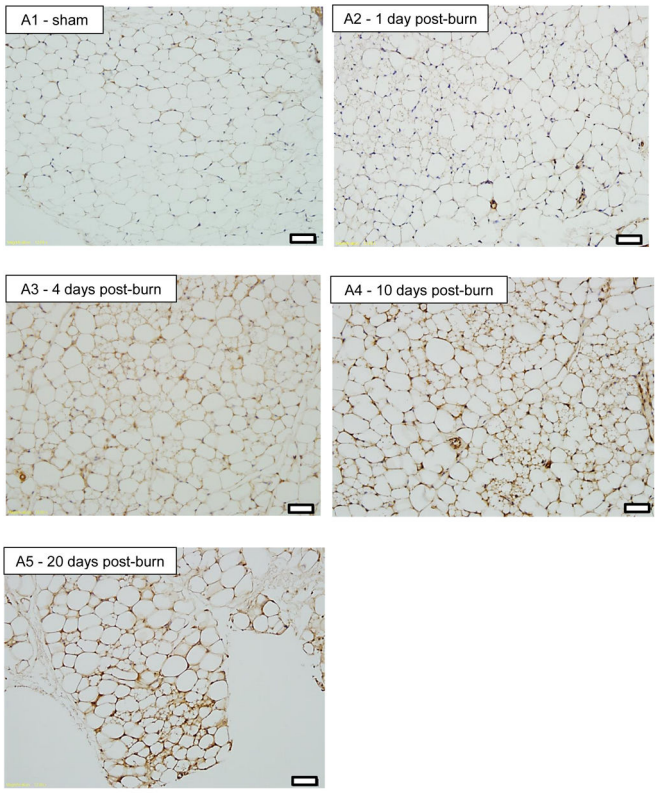

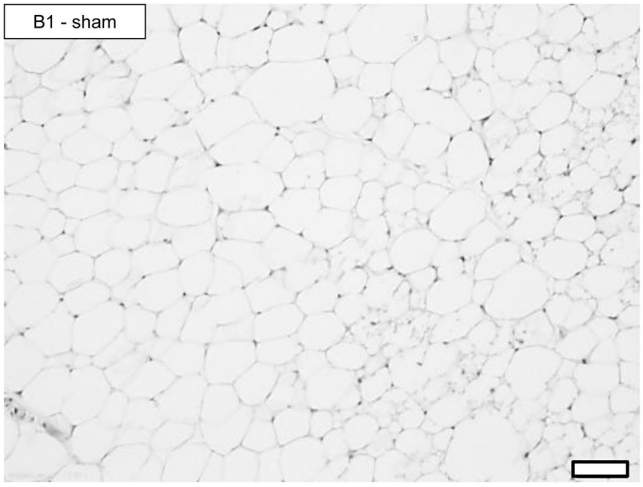

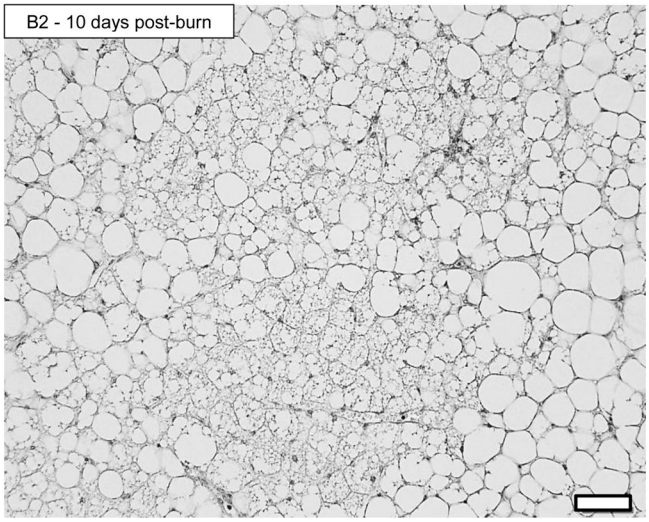

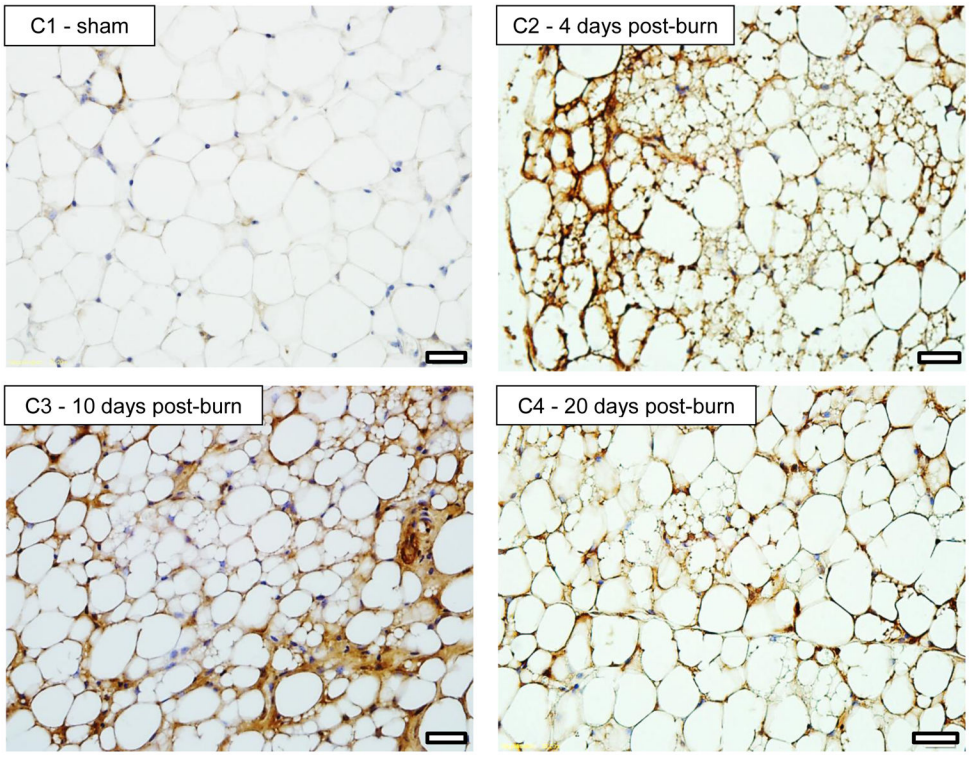

Figure 4.

20X histology of iWAT stained for UCP1 from sham (A1) and burned mice sacrificed at 1 (A2), 4 (A3), 10 (A4) and 20 (A5) days post injury showing induction of UCP1 protein. Black bars in the lower right corner of each picture represent 50μm. 20X histology of iWAT stained for UCP1 from sham (B1) and burned mice sacrificed at 10 days post injury (B2) showing a plethora of small multilocular adipocytes post burn, a feature of thermogenic adipose tissue. Black bars in the lower right corner of each picture represent 50μm. 40X histology of iWAT stained for UCP1 from sham (C1) and burned mice sacrificed at 4 (C2), 10 (C3) and 20 (C4) days post injury showing UCP1 staining within multilocular adipocytes. Black bars in the lower right corner of each picture represent 20μm.